

**Article Citation Format**

Alagbe, O.O. (2026): Non-Contact Body Temperature Monitoring Using Low-Cost Thermal Cameras in Smart Home Environments: An Experimental Study and Prototype Implementation. Journal of Digital Innovations & Contemporary Research in Science, Engineering & Technology.  
Vol. 14, No. 1. Pp 57-70. www.isteams.net/digitaljournal  
dx.doi.org/10.22624/AIMS/DIGITAL/V14N1P4

**Article Progress Time Stamps**

Article Type: Research Article  
Manuscript Received: 7<sup>th</sup> January, 2026  
Review Type: Blind Peer  
Final Acceptance: 3<sup>rd</sup> March, 2026

# Non-Contact Body Temperature Monitoring Using Low-Cost Thermal Cameras in Smart Home Environments: An Experimental Study and Prototype Implementation

**Oluwatobi Olukunle Alagbe**  
Department of Computer Science  
Aberystwyth University, Aberystwyth, Wales, UK  
E-mail: tobeea2017@gmail.com  
Phone NO: +447760941428

## ABSTRACT

This paper investigates the feasibility of using low-cost thermal cameras for continuous, non-contact body temperature monitoring within a smart home environment. Three thermal imaging devices were evaluated: two MLX90640 sensor modules mounted on different breakout boards (Pimoroni MLX-P and RobotShop MLX-R) and the RS PRO T-10 (RS-T10). Experiments were conducted in a controlled smart home laboratory with 30 participants across distances of 1 to 5 metres and ambient temperatures ranging from 16 °C to 25 °C. Physical factors, including skin colour emissivity, eyeglass use, and illumination source, were systematically assessed. Results demonstrate that ambient temperature and measurement distance are the dominant sources of measurement error, whereas skin emissivity and illumination type have a negligible impact. A bilinear interpolation compensation model was developed and integrated into a Three-Level Smart Home Architecture (3-LSHA), producing estimated body temperature values with an acceptable deviation from baseline readings across all tested conditions. A prototype system was implemented to demonstrate end-to-end well-being monitoring across multiple rooms. The findings confirm that low-cost thermal cameras, when coupled with appropriate compensation algorithms, are viable sensors for ambient-assisted living applications targeting body temperature trend monitoring and health alerting.

**Keywords:** Ambient Assisted Living, Bilinear Interpolation, Body Temperature Monitoring, Illumination Infrared Thermography, MLX90640, Smart Home, Thermal Camera, Well-Being Monitoring.

---

## 1. INTRODUCTION

The global demographic shift toward an ageing population has intensified demand for scalable technologies that support independent living. Ambient Assisted Living (AAL) systems aim to provide unobtrusive monitoring and intervention within domestic environments, enabling older adults to remain safely in their homes while reducing the burden on formal healthcare services [1], [2].

A fundamental physiological parameter in this context is body temperature, which is a primary indicator of fever, hypothermia, and general health status. Conventional contact thermometry is unsuitable for continuous, passive monitoring because it requires direct interaction with the subject. Thermal imaging cameras offer a compelling alternative by detecting infrared radiation emitted by the human body and computing surface temperature without physical contact. Recent miniaturisation and cost reduction of thermal sensors, exemplified by the Melexis MLX90640 family, have brought this technology within reach of consumer smart home deployments. Nevertheless, the performance of such devices under realistic domestic conditions, including varying distances, ambient temperatures, lighting environments, and human physiological diversity, remains incompletely characterised in the literature.

This paper addresses that gap through a structured experimental study conducted in the Smart Home Laboratory. The contributions of this work are fourfold:

- 1) A comparative evaluation of three thermal cameras (MLX-P, MLX-R, RS-T10) across distances of 1–5 m and six ambient temperature setpoints (16–25 °C) with 30 participants.
- 2) Systematic investigation of physical confounding factors: skin emissivity (skin colour), eyeglass use, and illumination source.
- 3) A bilinear interpolation compensation model that corrects raw thermal readings for ambient temperature and distance, integrated into a three-level smart home software architecture.
- 4) A multi-room prototype demonstration validating the end-to-end architecture under a realistic daily-activity scenario.

The remainder of this paper is organised as follows. Section II reviews related work. Section III describes the Three-Level Smart Home Architecture. Section IV details the experimental design and methodology. Section V presents results and analysis. Section VI describes the prototype implementation. Section VII discusses findings, limitations, and future directions. Section VIII concludes the paper.

## 2. RELATED WORKS

Thermal imaging has been applied to contactless temperature screening in a variety of clinical and public health settings. Studies following the COVID-19 pandemic demonstrated that IR cameras could screen febrile individuals at entry points with reasonable accuracy when environmental conditions were controlled [3], [4]. However, these deployments primarily targeted high-throughput screening at short, fixed distances and did not address the variable distances and ambient temperatures characteristic of domestic environments. In the AAL domain, sensor fusion approaches combining thermal, depth, and RGB-D cameras have been explored for fall detection and activity recognition [5], [6]. Body temperature monitoring using thermal cameras integrated into smart home platforms has received comparatively less attention. Prior work has largely focused on research-grade thermographic equipment with high spatial resolution, which is cost-prohibitive for widespread domestic deployment [7].

Low-cost thermal arrays such as the Melexis MLX90640 (32×24 pixels) and the FLIR Lepton series have been evaluated for fever detection and occupancy estimation [8]. Existing studies generally report measurements at close range ( $\leq 1$  m) and under controlled ambient conditions, leaving a gap regarding performance across the 1–5 m range relevant to room-scale smart home deployments.

This work directly addresses that gap by systematically evaluating temperature compensation strategies across varied distances and ambient conditions, and by embedding the resulting model into a full software architecture prototype.

### **3. THREE-LEVEL SMART HOME ARCHITECTURE (3-LSHA)**

The Three-Level Smart Home Architecture (3-LSHA) provides the software framework into which the thermal camera monitoring subsystem is integrated. The architecture is organised into three hierarchical levels, as described below.

#### **A. Sensor Level**

The sensor level abstracts all physical sensing devices through an object-oriented sensor class hierarchy. Each sensor subclass exposes a standardised interface providing timestamp, location, sensor identifier, and data payload. Thermal cameras are represented as Camera Sensor subclasses returning a two-dimensional temperature array. Ambient temperature sensors (e.g., DHT11/DHT22) and distance sensors (infrared ranging modules) complement the thermal camera data at this level. All sensor readings are published to an event bus and logged to a central diary database.

#### **B. Processing Level**

The processing level receives raw sensor data and applies domain-specific algorithms. For body temperature monitoring, an Immediate Processor subclass implements the bilinear interpolation compensation model (Section V-C) and evaluates estimated temperature against an adaptive statistical threshold. Additional processor subclasses handle CO<sub>2</sub>-based occupancy estimation and ambient temperature comparison. The processor level is designed for extensibility: new processor types can be added without modifying existing components, consistent with the Open/Closed Principle.

#### **C. Action Level**

The action level executes responses determined by the processing level. Relevant action subclasses for body temperature monitoring include Robot Action (dispatching a mobile robot for contact thermometer verification), Control Heating System Action (adjusting the HVAC system), Communication Action (notifying family members or a general practitioner via VoIP or text message), and Window Action (opening windows to improve ventilation). All triggered actions are logged to the system diary with timestamps and location identifiers.

#### **D. Body Temperature Monitoring Use Case**

The body temperature monitoring use case operates on a ten-minute polling cycle. At each cycle, the thermal camera in the room currently occupied by the subject captures a peak forehead temperature reading  $t_h$ . The processing level applies the compensation model to derive a corrected estimate and compares it against the adaptive range  $[t_m - t_\sigma, t_m + t_\sigma]$ . Normal readings trigger routine diary logging. Abnormal readings escalate through the action hierarchy: first dispatching a contact-measurement robot, then notifying caregivers if confirmed, and simultaneously adjusting the HVAC system.

## 4. EXPERIMENTAL METHODOLOGY

### A. Equipment

Three thermal imaging devices were selected for evaluation, as detailed in Table I. The Pimoroni MLX90640 (MLX-P) and RobotShop MLX90640 (MLX-R) are both based on the Melexis MLX90640 sensor die and produce 32×24 pixel thermal images at up to 64 Hz with a stated accuracy of ±1°C. The RS PRO T-10 (RS-T10) offers substantially higher spatial resolution (206×156 pixels) and a ±5°C accuracy specification, with a narrower field of view. At the time of the study, the approximate retail prices were £60.00 (MLX-P), £62.34 (MLX-R), and £262.14 (RS-T10). All three cameras are capable of operating within the domestic ambient temperature range of 16°C to 40°C and can detect subjects within the 1–5 m range relevant to room-scale deployments.

### Thermal Camera Specifications

**Table 1: Thermal cameras specification table**

Specification	MLX90640 (MLX-P / MLX-R)	RS PRO T-10 (RS-T10)
Resolution	32 × 24 pixels	206 × 156 pixels
Field of View	110° × 75°	26.8° × 35°
Refresh Rate	16 Hz – 64 Hz	9 Hz
Operating Temp.	–40°C to 85°C	–20°C to 60°C
Measurement Range	–40°C to 300°C	–10°C to 330°C
Power Supply	3.3 V and 5 V	3.3 V and 5 V
Detection Range	136.5 m	330 m
Accuracy	±1°C	±5°C
Approximate Cost	£60 / £62.34	£262.14

### B. Laboratory Setup

All experiments were conducted in the Smart Home Laboratory. The three cameras were mounted simultaneously on an adjustable tripod stand, ensuring a consistent angle toward the subject's forehead. Each camera was connected to a dedicated display monitor. The display rendered a colour-coded or greyscale thermal image with an automatic peak-temperature crosshair overlay indicating the hottest detected point. Participants were seated on an upright dining chair with their shoulders aligned and neck in a neutral, straight posture to maximise forehead exposure. No specific clothing protocol was enforced to replicate real-world conditions where occupants dress according to comfort. A medical-grade clinical thermometer was used to record a baseline (control) body temperature for each participant immediately before thermal camera measurement. Baseline readings at the time of the experiment were 35.6°C, 36.4°C, and 36.9°C for the three pilot participants. Distance markers were placed on the floor at 1, 2, 3, 4, and 5 metres from the camera plane (Fig. 1). Ambient temperature in the laboratory was monitored continuously using a calibrated sensor, and sessions were suspended if the ambient temperature drifted beyond the target setpoint band. Data were captured in short, consecutive windows to minimise physiological temperature fluctuations in participants.

### **C. Pilot Experiment: Physical Factor Assessment**

A preliminary experiment with three volunteer participants (two with light skin, one with dark skin; two eyeglass users, one non-user) was conducted to examine the influence of four physical factors on thermal camera readings:

- 1) Skin emissivity (operationalised via skin colour: light vs. dark).
- 2) Eyeglass use (with eyeglasses vs. without eyeglasses).
- 3) Illumination source (artificial LED vs. natural daylight through open window blinds).
- 4) Ambient temperature (16°C, 20°C, and 26°C setpoints).

All other variables were held constant during each comparison. Measurements were acquired at distances of 1, 2, 3, 4, and 5 metres for each scenario combination.

### **D. Extended Experiment: 30-Participant Study**

Following the pilot, an expanded study was conducted with 30 participants across six ambient temperature setpoints: 16°C, 18°C, 20°C, 22°C, 24°C, and 25°C. Sessions were distributed over three days to achieve the required ambient temperature variation, with morning sessions targeting 16°C, 20°C, and 24°C, and afternoon sessions targeting 22°C, 18°C, and 25°C. Participants were both eyeglass users and non-users. For each participant, readings were recorded at 1, 2, 3, 4, and 5 metres for all three cameras.

## **5. RESULTS AND ANALYSIS**

### **A. Skin Emissivity (Skin Colour)**

Comparison of thermal camera readings between light-skinned and dark-skinned subjects, as seen in Figure 1, revealed minimal inter-group variation across all three cameras. This finding is consistent with the established biophysical literature, which reports a mean human skin emissivity of 0.97 (range 0.96–0.99) that is independent of melanin pigmentation [9]. The MLX-P and MLX-R cameras consistently recorded slightly higher values compared to the RS-T10, regardless of the subject's skin tone. Both camera types exhibited a linear decrease in recorded temperature with increasing subject distance. The minor inter-subject temperature differences observed (approximately 0.3°C maximum) can plausibly be attributed to the differing actual baseline temperatures of the volunteers (35.6°C and 36.9°C) rather than to skin emissivity per se. These results support the hypothesis that skin colour does not constitute a meaningful confound for thermal camera-based body temperature estimation in this context. Accordingly, skin type was not treated as a correction variable in the subsequent compensation model.

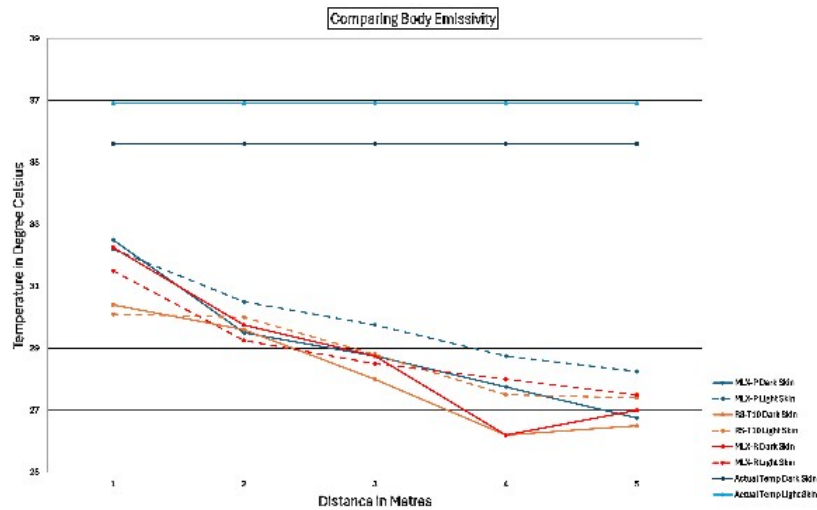


**Figure 1 Skin Emissivity Comparison**

**B. Eyeglass Use**

The pilot experiment suggested that eyeglass frames might occlude forehead regions and affect readings at longer distances due to pixel-level averaging effects. However, the extended 30-participant study found that the impact was negligible across all three cameras. The mean temperature difference between with-glasses and without-glasses conditions was 0.3°C (SD = 0.15°C) for the MLX-P, 0.2°C (SD = 0.13°C) for the MLX-R, and 0.2°C (SD = 0.16°C) for the RS-T10. These differences are within the manufacturer's stated accuracy specifications. The findings indicate that eyeglass use does not significantly impair thermal camera readings at distances of 1–5 m and therefore does not require separate compensation. This is practically important for AAL deployments because it is infeasible to require occupants to remove eyeglasses for routine monitoring.

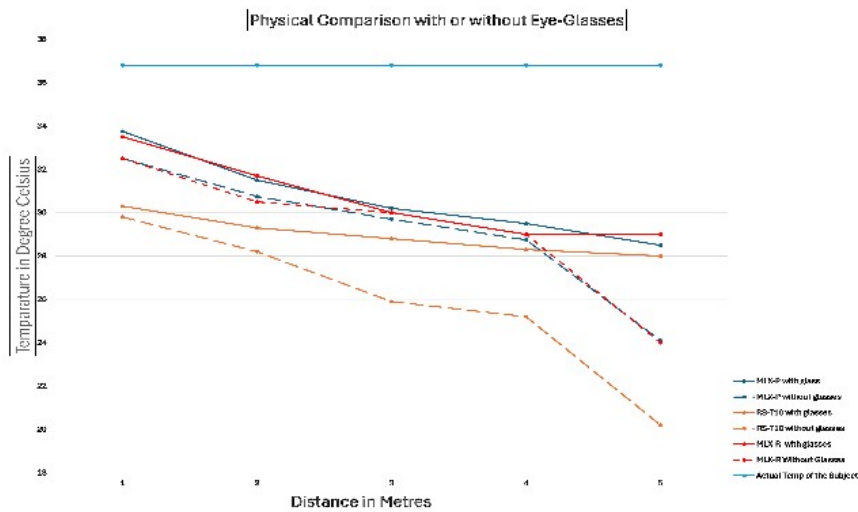


**Figure 2: Comparison With or Without Eyeglasses**

### C. Illumination Source

Temperature readings obtained under artificial LED illumination and natural daylight were statistically comparable across all three cameras, with differences within the cameras' measurement uncertainty bands. This result is expected from first principles: thermal cameras operate in the 8–14 μm long-wave infrared band and are insensitive to visible-spectrum illumination. LED bulbs emit negligible infrared

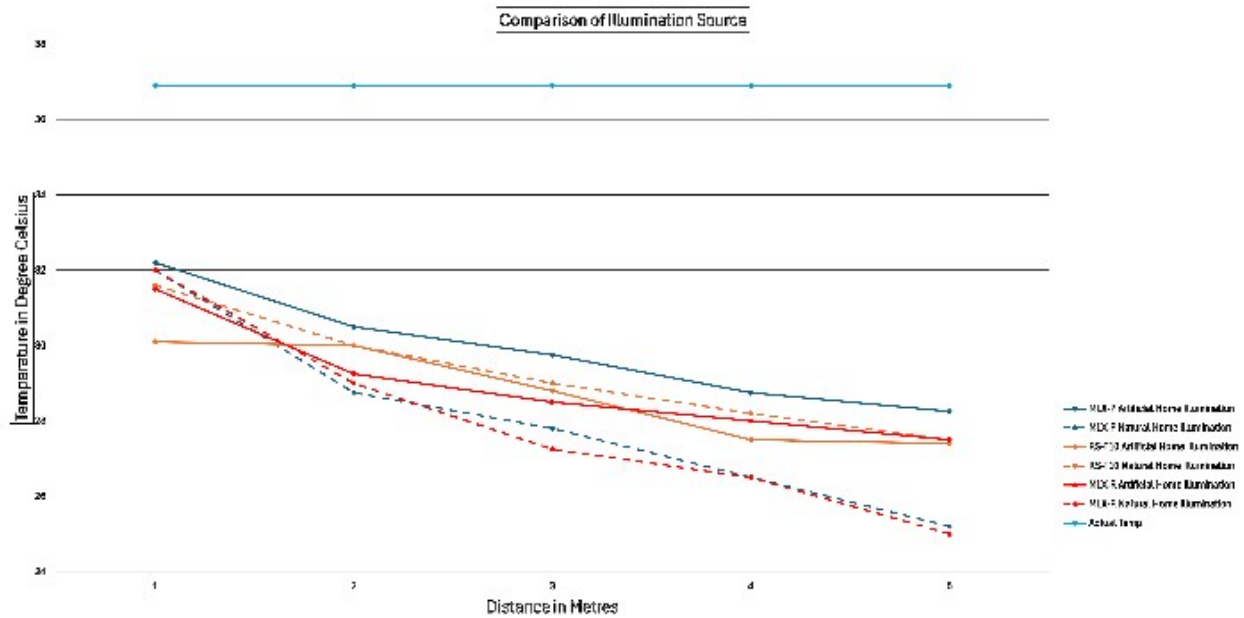


**Figure 3: Comparing Illumination Source Energy in this Band.**

The experiment confirms that domestic lighting arrangements do not require compensation in body temperature estimation algorithms, simplifying real-world deployment.

### D. Ambient Temperature and Distance Effects

Ambient temperature and measurement distance were identified as the two dominant confounding factors. As distance increased from 1 m to 5 m, all three cameras exhibited a monotonically decreasing average temperature reading, consistent with the inverse relationship  $T \propto 1/d$ , where  $T$  is the recorded temperature and  $d$  is the camera-to-subject distance. This effect arises because thermal energy emitted by the subject is dispersed over a progressively larger solid angle, reducing the irradiance at the camera sensor. At the pixel level, the camera increasingly captures a mixture of skin and background pixels at greater distances, biasing the peak reading toward the lower background temperature. Standard deviation of repeated readings also increased with distance: for the MLX-P, SD ranged from 0.9°C at 1 m to 2.2°C at 5 m; for the MLX-R, from 1.0°C to 2.3°C; and for the RS-T10, from a lower baseline to a higher upper extreme. The RS-T10 exhibited greater variability at distances above 2 m compared to the MLX cameras, despite its higher spatial resolution, possibly due to its narrower field of view requiring more precise subject alignment.

Ambient temperature effects were most pronounced at distances  $\geq 3$  m. At 1 m, all cameras showed standard deviations across the six ambient temperature setpoints of less than  $0.3^{\circ}\text{C}$  (RS-T10:  $0.15^{\circ}\text{C}$ ; MLX-R:  $0.21^{\circ}\text{C}$ ; MLX-P:  $0.24^{\circ}\text{C}$ ). At 5 m, variability increased substantially (RS-T10:  $0.70^{\circ}\text{C}$ ; MLX-R:  $0.95^{\circ}\text{C}$ ; MLX-P:  $1.12^{\circ}\text{C}$ ). Afternoon measurement sessions consistently produced slightly lower readings than morning sessions at matching ambient temperatures, suggesting that uncontrolled extraneous variables such as clothing insulation, hydration, or cumulative physical activity contributed to within-session variability. Three-dimensional trend surface plots of measured temperature as a function of distance and ambient temperature confirmed a smooth, monotonic response surface for all three cameras, validating the use of a bilinear interpolation model to characterise and correct these two confounds jointly.

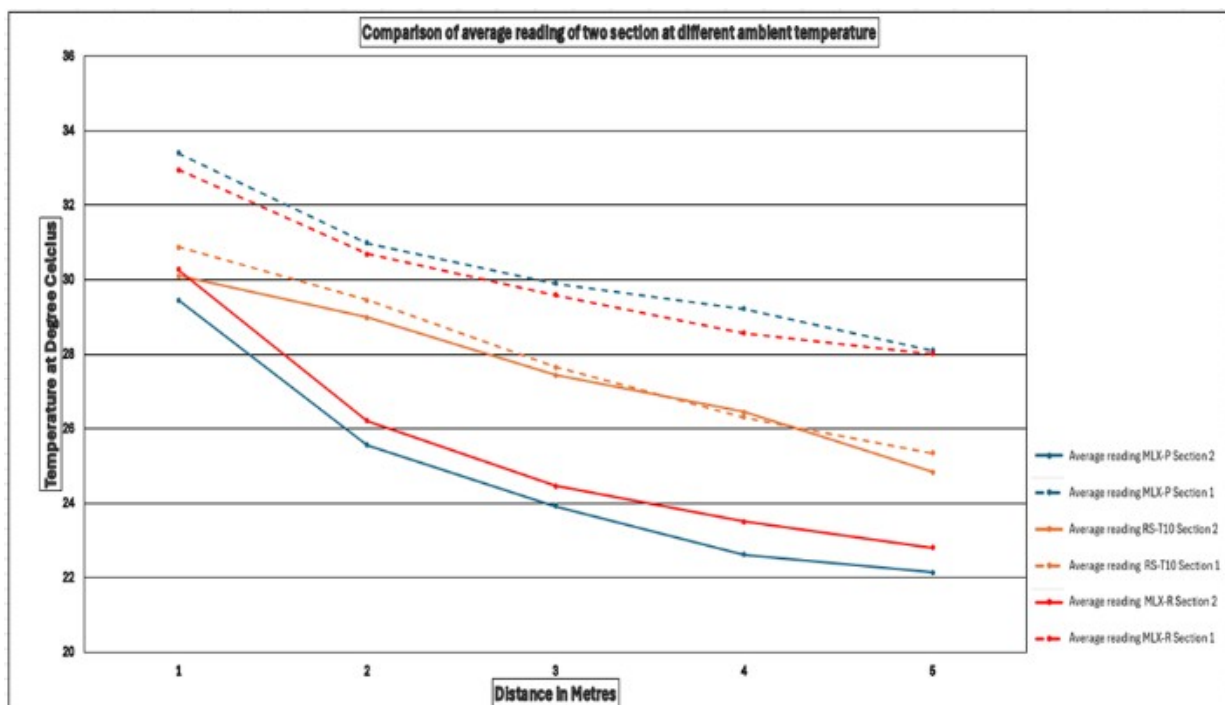


**Figure 4: Comparing Ambient Temperature**

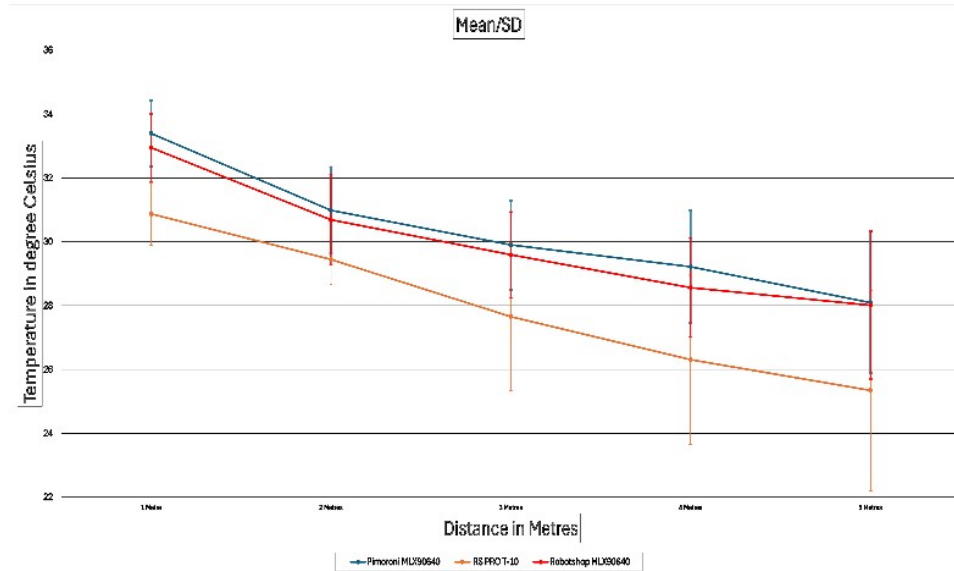


**Figure 5: Effect of Distance**

### E. Bilinear Interpolation Compensation Model

Bilinear interpolation estimates unknown values on a regular two-dimensional grid using the four nearest known data points, producing a smooth surface that accounts for both axes simultaneously. In this application, the grid axes are ambient temperature ( $T_a$ ) and distance ( $d$ ), and the interpolated value is the expected mean camera reading  $t_m$  for a subject with normal body temperature. The standard deviation  $t_\sigma$  across repeated measurements at each ( $T_a$ ,  $d$ ) combination is also stored in the look-up table. Given a real-time measurement triplet ( $t_h$ ,  $T_a$ ,  $d$ ), the processing level retrieves  $t_m$  and  $t_\sigma$  by bilinear interpolation and applies the acceptance criterion:

$$t_m - t_\sigma \leq t_h \leq t_m + t_\sigma \quad (1)$$

If the measured temperature  $t_h$  falls within this range, the reading is classified as normal and logged to the diary. If  $t_h$  exceeds the upper bound or falls below the lower bound, the reading is classified as abnormal, and the action hierarchy is engaged. The magnitude and direction of the deviation can be used to distinguish mild anomalies (temperature slightly above normal) from severe anomalies (fever threshold exceeded), enabling proportionate responses.

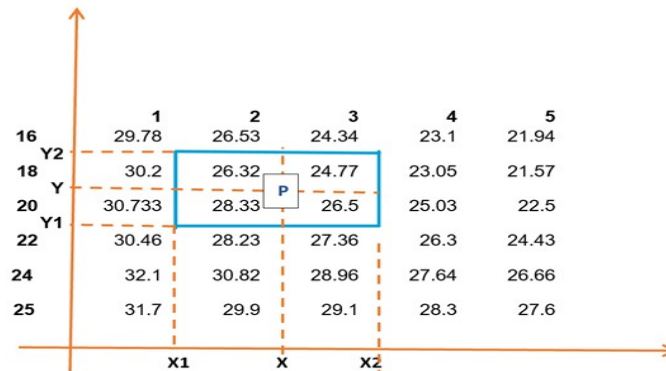


Figure 6: The Bi-linear interpolation

## 6. PROTOTYPE IMPLEMENTATION AND SCENARIO DEMONSTRATION

### A. System Design Overview

A software prototype of the 3-LSHA was developed to demonstrate end-to-end body temperature monitoring within a simulated multi-room home environment. The prototype is structured around four functional blocks: the Sensor Block, the Processor Block, the Action Block, and the Diary and Reports Block. The scenario models the daily activities of a hypothetical 65-year-old resident (Mr3 X) living independently in a single-storey home measuring 12.0 × 10.0 m, comprising a bedroom, dining room, lounge, and kitchen, arranged around a 2.0 m cross-shaped hallway. Each room has an internal footprint of 5.0 × 4.0 m. MLX-P thermal cameras, CO<sub>2</sub> sensors, and ambient temperature sensors are mounted at the upper corner of each room.

### B. Sensor Block

The Sensor Block uploads pre-arranged CSV files representing sensor readings at fixed time intervals (CO<sub>2</sub> and ambient temperature every 10 minutes; body temperature once per hour). Each record includes a timestamp, room identifier, and sensor data fields. For the prototype demonstration, hypothetical data were generated to represent plausible readings across a full active day (07:00–23:00). The sensor block validates schema integrity (expected column headers, data types, and absence of null values) before publishing records to the processing pipeline.

### C. Processor Block

Python scripts uploaded to the Processor Block query the sensor data, load them into memory, and execute the following analytical steps:

- 1) Body temperature estimation: bilinear interpolation over (T<sub>a</sub>, d) to obtain t<sub>m</sub> and t<sub>σ</sub>; threshold comparison to classify each hourly reading.
- 2) Ambient temperature monitoring: comparison against a comfort band of 20–22 °C; activation of window or cooling actions on threshold breach.

### D. Action Block and Diary

The Action Block presents six programmable response modules: window action, door action, cooling system action, robot action (contact measurement dispatch), communication action (family/GP notification), and diary update. Actions are triggered automatically by the Processor Block, logged with timestamps and room locations to the append-only diary, and displayed as an action timeline in the prototype interface.

The Diary and Reports Block provides interactive functions: view graph (data and process result visualisation), action timeline display, diary clearing, and report export. All generated reports are made available for download from the interface.

### E. Use-Case Scenario Results

Table II presents the hourly body temperature processing results for Mr X across eight monitoring events from 07:00 to 14:00, illustrating the system's end-to-end decision logic.

**TABLE II**

**Body Temperature Monitoring Results – Mr X Scenario (Hypothetical Data)**

Time	Room	Amb. Temp (°C)	Distance (m)	Meas. Temp (°C)	Mean Temp (°C)	Acceptable Range (°C)	Status / Action
07:00	Bedroom	23.9	1.1	32.1	31.89 ± 0.59	30.71 – 33.06	Normal – Routine logging
08:00	Kitchen	24.0	3.0	28.96	28.96 ± 1.03	26.91 – 31.01	Normal – Routine logging
09:00	Living Room	25.2	5.1	27.65	27.79 ± 0.40	26.98 – 28.59	Normal – Routine logging
10:00	Study Room	25.7	4.5	32.0	28.57 ± 0.32	27.94 – 29.21	Abnormal – Open window, dispatch robot
11:00	Study Room	26.0	3.0	32.5	29.24 ± 0.67	27.90 – 30.58	Abnormal – Alert GP
12:00	Living Room	26.5	2.9	32.1	29.23 ± 0.53	28.17 – 30.29	Abnormal – Alert family
13:00	Living Room	26.7	2.5	31.8	28.84 ± 0.28	28.27 – 29.40	Abnormal – Adjust HVAC, dispatch robot
14:00	Bedroom	27.2	2.3	32.0	28.34 ± 0.05	28.24 – 28.44	Abnormal – Adjust HVAC

Table 2: Results of processed data of Mr X's activities

At 09:00 in the living room (distance 5.1 m, ambient 25.2°C), the interpolated mean  $t_m$  was 27.79°C with  $t_\sigma = 0.40$ °C, yielding an acceptable range of 26.98–28.59°C. The measured value  $t_h = 27.65$ °C fell within this range, and the reading was classified as normal. From 10:00 onwards, measured values rose sharply above the acceptable range (peak deviation of +3.43°C at 10:00 in the study room), indicating a simulated fever onset. The action hierarchy was progressively engaged: robot dispatch, GP alerting, family notification, and HVAC adjustment, with all events logged to the diary. The system returned to routine logging once readings normalised in the afternoon period of the full-day scenario(07:00–23:00).

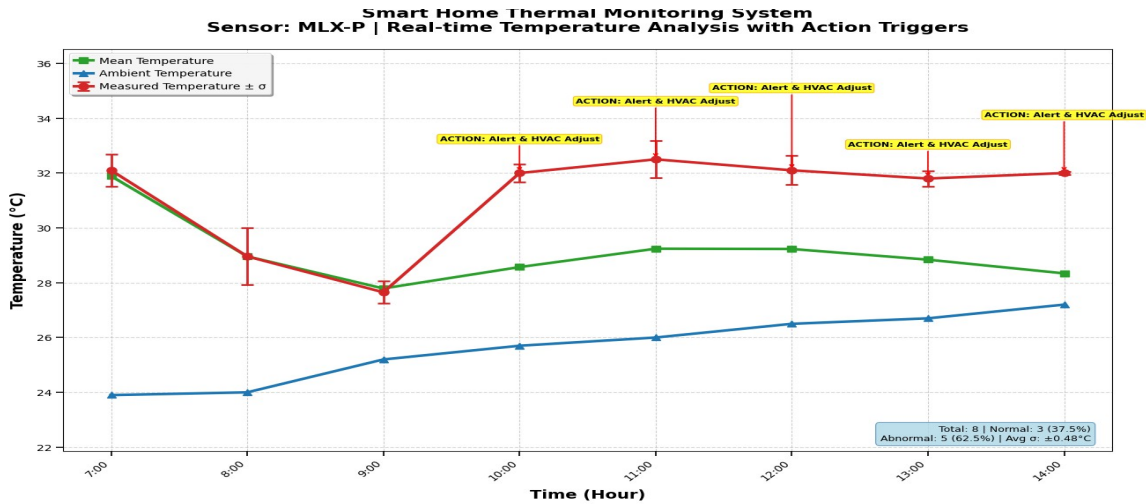


**Figure 7: Body Temperature Monitoring Result of Mr X**

## 7. DISCUSSION

### A. Key Findings

The experimental results confirm that low-cost thermal array cameras are technically viable for body temperature trend monitoring in smart home environments, provided that systematic compensation for ambient temperature and measurement distance is applied. The bilinear interpolation model provides a computationally inexpensive and practically effective mechanism for this correction. Among the physical factors assessed, only ambient temperature and distance produced statistically meaningful effects on readings; skin emissivity, illumination source, and eyeglass use had negligible impact and do not require dedicated compensation. The MLX-P and MLX-R cameras demonstrated better repeatability (lower SD across repeated measurements) compared to the RS-T10 despite their lower spatial resolution. This counterintuitive result may reflect the wider field of view of the MLX cameras, which provides more robust peak detection in the forehead region across the 1–5 m range, whereas the RS-T10's narrower field of view is more sensitive to slight misalignment. The substantially lower cost of the MLX90640 (approximately one-quarter that of the RS-T10) further supports its selection as the preferred sensor for cost-effective AAL deployments.

The maximum recorded body temperature by any thermal camera during the experiments was approximately 33 °C, which is below the normal physiological range of 36.6–37.0 °C. This systematic underestimation is an expected characteristic of non-contact surface temperature measurement, where conductive heat transfer pathways from the core to the skin surface and the microclimate layer between skin and camera introduce attenuation. The compensation model addresses this by treating interpolated mean values as relative indicators rather than absolute measures, comparing individual readings against a statistically derived normal range for each (T<sub>a</sub>, d) combination. This relative approach enables clinically meaningful classification (normal vs. abnormal trend) without requiring absolute accuracy at the level of a contact thermometer.

## **B. Limitations**

Several limitations must be acknowledged. First, distance measurement in the experiments was performed manually using floor markers; automated distance sensing (e.g., ultrasonic or time-of-flight modules) would reduce human measurement error and improve the reliability of the compensation model in deployment. Second, confounding factors such as clothing coverage, hair occluding the forehead, and cumulative physical activity before measurement were not fully controlled, and their influence on readings remains to be quantified. Third, the prototype demonstrated monitoring of a single occupant; scenarios involving multiple residents require multi-target tracking and individualised compensation, which were not addressed in this study. Fourth, the prototype operated on batch-processed CSV datasets rather than real-time asynchronous sensor streams; a full deployment would require integration with a live event bus and asynchronous data fusion pipeline. Finally, the long-term drift characteristics of the MLX90640 sensor under continuous operation in a domestic environment have not been assessed.

## **C. Future Work**

Future research should address the following directions. Integration of automated distance sensing (e.g., ultrasonic ranging or infrared time-of-flight modules) will eliminate manual distance measurement and enable dynamic compensation as occupants move. Machine learning approaches, particularly Gaussian process regression or neural network interpolation, may provide more accurate and generalisable compensation models than bilinear interpolation. A pan-tilt-zoom tracking camera fused with a fixed thermal camera could enable automatic subject following and hotspot localisation (targeting the forehead), improving accuracy and enabling multi-occupant monitoring. Longitudinal real-world trials with genuine older adult residents are essential to assess system reliability, user acceptance, and clinical utility over extended periods. Finally, integration of the thermal monitoring subsystem with other AAL modalities—including wearable pulse oximetry, bed pressure sensors, and door contact sensors—within the 3-LSHA framework would enable richer, cross-validated health status inference.

## **7. CONCLUSION**

This paper has presented a systematic experimental characterisation of low-cost thermal cameras for non-contact body temperature monitoring in smart home environments and has demonstrated their integration within a Three-Level Smart Home Architecture. Among three tested devices (MLX-P, MLX-R, and RS-T10), the MLX90640-based cameras provided superior repeatability at a substantially lower cost, making them the preferred choice for ambient-assisted living applications. Ambient temperature and measurement distance were confirmed as the primary sources of reading variability, and both were effectively compensated using a bilinear interpolation model embedded in the processing level of the architecture. Skin emissivity, eyeglass use, and illumination type were shown to have negligible influence on readings, simplifying the compensation pipeline. A functional prototype validated the end-to-end system, demonstrating automatic detection of simulated fever conditions, adaptive action triggering across the HVAC, robotic, and communication response modules, and comprehensive diary logging. The research establishes a practical framework for affordable, unobtrusive body temperature monitoring as a component of personalised well-being support for individuals living independently at home.

## REFERENCES

- [1] W. Rashid, A. Jabbar, and F. Al-Turjman, Ambient assisted living for the elderly: A survey, *IEEE Access*, vol. 9, pp. 59355-59373, 2021.
- [2] J. C. Augusto, Ambient intelligence: The confluence of ubiquitous/pervasive computing and artificial intelligence, *Intell. Comput. Everywhere*, pp. 213-234, 2007.
- [3] A. Bhatt, B. Patel, and M. Shah, Infrared thermal imaging for COVID-19 fever screening: Challenges and prospects, *Sensors*, vol. 21, no. 12, Art. no. 4109, 2021.
- [4] F. Ring, Thermal imaging today and its relevance to diabetes, *J. Diabetes Sci. Technol.*, vol. 4, no. 4, pp. 857-862, 2010.
- [5] L. Bian, E. Andersen, M. Marks, D. Yabsley, and R. Saunders, Fall detection using thermal sensors and deep learning, *Sensors*, vol. 22, no. 5, Art. no. 1972, 2022.
- [6] P. Ni, C. Zhang, and D. Gao, Activity recognition using thermal depth cameras in smart home environments, *IEEE Trans. Autom. Sci. Eng.*, vol. 18, no. 2, pp. 740-751, 2021.
- [7] S. Cho, J. Park, and Y. Lee, A review of thermal imaging for human activity analysis in smart homes, *Sensors*, vol. 20, no. 20, Art. no. 5750, 2020.
- [8] M. Dzaferovic, A. Sokic, and E. Sokic, Low-cost thermal imaging for occupancy detection and fever screening, *Electronics*, vol. 10, no. 15, Art. no. 1774, 2021.
- [9] P. Togawa, T. Tamura, and O. Enberg, *Biomedical Transducers and Instruments*, CRC Press, Boca Raton, FL, USA, 1997.